

Performance enhancement of a viscoelastic bistable energy harvester using time-delayed feedback control

Mei-Ling Huang(黄美玲), Yong-Ge Yang(杨勇歌), and Yang Liu(刘洋)

Citation: Chin. Phys. B, 2024, 33 (**6**): 060203. DOI: 10.1088/1674-1056/ad3b89
Journal homepage: http://cpb.iphy.ac.cn; http://iopscience.iop.org/cpb

What follows is a list of articles you may be interested in

Research and application of composite stochastic resonance in enhancement detection

Rui Gao(高蕊), Shangbin Jiao(焦尚彬), and Qiongjie Xue(薛琼婕)
Chin. Phys. B, 2024, 33 (**1**): 010203. DOI: 10.1088/1674-1056/ad01a8

Dynamic responses of an energy harvesting system based on piezoelectric and electromagnetic mechanisms under colored noise

Yong-Ge Yang(杨勇歌), Yun Meng(孟运), Yuan-Hui Zeng(曾远辉), and Ya-Hui Sun(孙亚辉)
Chin. Phys. B, 2023, 32 (**9**): 090201. DOI: 10.1088/1674-1056/acd621

Sparse identification method of extracting hybrid energy harvesting system from observed data

Ya-Hui Sun(孙亚辉), Yuan-Hui Zeng(曾远辉), and Yong-Ge Yang(杨勇歌)
Chin. Phys. B, 2022, 31 (**12**): 120203. DOI: 10.1088/1674-1056/ac9cbf

Stochastic response of van der Pol oscillator with two kinds of fractional derivatives under Gaussian white noise excitation

Yong-Ge Yang(杨勇歌), Wei Xu(徐伟), Ya-Hui Sun(孙亚辉), Xu-Dong Gu(谷旭东)
Chin. Phys. B, 2016, 25 (**2**): 020201. DOI: 10.1088/1674-1056/25/2/020201

Response of a Duffing—Rayleigh system with a fractional derivative under Gaussian white noise excitation

Zhang Ran-Ran (张冉冉), Xu Wei (徐伟), Yang Gui-Dong (杨贵东), Han Qun (韩群)
Chin. Phys. B, 2015, 24 (**2**): 020204. DOI: 10.1088/1674-1056/24/2/020204

Performance enhancement of a viscoelastic bistable energy harvester using time-delayed feedback control

Mei-Ling Huang(黄美玲)[1], Yong-Ge Yang(杨勇歌)[1,2,†], and Yang Liu(刘洋)[3]

[1] *School of Mathematics and Statistics, Guangdong University of Technology, Guangzhou* 510520, *China*
[2] *State Key Laboratory for Strength and Vibration of Mechanical Structures, Xi'an Jiaotong University, Xi'an* 710049, *China*
[3] *Exeter Small-Scale Robotics Laboratory, Engineering Department, University of Exeter, North Park Road, Exeter EX*4 4*QF, UK*

(Received 8 March 2024; revised manuscript received 28 March 2024; accepted manuscript online 7 April 2024)

This paper focuses on the stochastic analysis of a viscoelastic bistable energy harvesting system under colored noise and harmonic excitation, and adopts the time-delayed feedback control to improve its harvesting efficiency. Firstly, to obtain the dimensionless governing equation of the system, the original bistable system is approximated as a system without viscoelastic term by using the stochastic averaging method of energy envelope, and then is further decoupled to derive an equivalent system. The credibility of the proposed method is validated by contrasting the consistency between the numerical and the analytical results of the equivalent system under different noise conditions. The influence of system parameters on average output power is analyzed, and the control effect of the time-delayed feedback control on system performance is compared. The output performance of the system is improved with the occurrence of stochastic resonance (SR). Therefore, the signal-to-noise ratio expression for measuring SR is derived, and the dependence of its SR behavior on different parameters is explored.

Keywords: energy harvesting, bistability, stochastic averaging method, stochastic resonance, time-delayed feedback control

PACS: 02.50.–r, 05.40.–a, 05.40.Ca **DOI:** 10.1088/1674-1056/ad3b89

1. Introduction

The sustainable development of society requires the support of energy, while traditional energy obviously cannot meet the long-term development demand, which means that the search and exploration of sustainable energy is inevitable. With the digging of sustainable energy, it is noticed that vibration is ubiquitous in the environment.[1,2] Therefore, the vibration energy harvesting technique has attracted extensive attention. With the rapid development of self-supplied electronic equipment with low energy consumption, vibration energy harvesting has been utilized in many fields in recent years, such as biomedical field, environmental monitoring field and mechanical engineering field.[3–5] The earliest proposed linear energy harvesting system is appropriate to work under narrow-band excitation, while the energy conversion efficiency is unsatisfactory when the vibration energy source is in a wide frequency spectrum.[6,7] For improving the working efficiency of energy harvester and broadening its working frequency bandwidth, various nonlinear energy harvesting systems have been proposed and designed successively which mainly involve impact,[8,9] monostable Duffing,[10,11] and bistable oscillator.[12,13]

Among them, the bistable oscillator will produce periodic inter-well vibration due to the special double-well restoring force potential, which can effectively promote the performance of energy collection system.[14] Meanwhile, as the bistable oscillator is adopted, there is no requirement for the frequency and vibration form of external excitation, which enhances the deficiency that the linear energy harvester is only applicable to a narrow frequency spectrum.[15] Accordingly, the research on bistable energy harvesting attracts many scholars. Stanton *et al.*[16] verified the inherent adaptability of nonlinear system with excellent performance in practical application by a bistable oscillator constructed by piezoelectric cantilever and permanent magnet. Cohen *et al.*[17] applied slow-fast decomposition to assess the dynamic of bistable energy harvesting system under low frequency excitation, and made an effort to solve the asymmetry of restoring force potential of bistable energy harvesting system. Liu *et al.*[18] designed a new bistable energy harvester based on the amplified piezoelectric structure, and provided a approach to explore the inter-well motion through frequency spectrum. The research of Zheng *et al.*[19] focused on the performance optimization analysis and experimental research of bistable energy harvester due to SR behavior. Wang *et al.*[20] adopted the configuration of elastic amplifier to enhance the basic excitation for providing sufficient kinetic energy to jump over the potential well barrier of large-amplitude bistable motion, and analyzed the response and productivity characteristics of the proposed system by simulation and experiment. Yousefpour *et al.*[21] utilized the input saturation terminal sliding mode control method based on disturbance observer in bistable piezomagnetoelastic energy harvester to achieve the control of switching different attractors of vibration energy harvesting system. In

[†]Corresponding author. E-mail: yonggeyang@163.com

© 2024 Chinese Physical Society and IOP Publishing Ltd

addition, the time-delay that widely exists in natural and practical applications and often hinders the stability of the system makes it necessary to introduce time-delayed feedback control into the energy harvesting system.[22]

Despite the fact that time delay is generally used to suppress the large-amplitude vibration of the system, it can also enlarge the resonance amplitude and further promote the system performance under some appropriate time delay parameters.[23–26] Huan *et al.*[27] proposed a new approach to determine the asymptotic stability of quasi-integrable Hamiltonian systems with random time delay control, and provided a two-degree-of-freedom networked control system driven by Gaussian white noise under random time delay control to verify the applicability and effectiveness of the proposed approach. Xu *et al.*[28] analyzed the SR of a delayed tristable system excited by harmonic signals and correlated noises, and found that proper time delay is beneficial to enhance SR and increase system output. Yang and Cao[29] studied the stochastic response and SR of hybrid energy harvesting system under the control of time-delay feedback, and found that time-delayed feedback can improve the performance of hybrid energy harvesting system and enhance the SR phenomenon of the system. Zhang *et al.*[30] applied time-delay feedback control in nonlinear piezoelectric energy harvester driven by additive and multiplicative white Gaussian noise to improve system performance. De and Ali[31] investigated the broadband energy harvesting of bistable energy harvester with sufficient power output, and adopted time-delayed feedback control to upgrade the efficiency of energy harvester.

Furthermore, the improvement and perfecting of the energy harvester can be achieved not only by oscillator design and control methods, but also by application of advanced material that has viscoelastic behavior[32] and the proper use of the dynamics of the system. Viscoelastic material has been applied in physics, medicine, engineering, mathematics, and other fields because of its unique characteristics of stress relaxation, creep, energy storage, and dissipation.[33–36] Oumbé Tékam *et al.*[37] focused on the dynamics of fractional viscoelastic materials applied to a strong nonlinear energy harvesting system, and analyzed the complexity of system response by controlling viscoelastic parameters. According to research by Huang *et al.*,[38] the relationship between the parameters of the tristable viscoelastic vibration isolation system under random excitation and the dynamic characteristics of system under the time-delayed feedback control was established. Tuwa *et al.*[39] analyzed the dynamics of a quarter automobile suspension with a fractional derivative viscoelastic model, and explored the dependence of the amplitude of a quarter automobile suspension model on viscoelastic parameters. Yang *et al.*[40] investigated the stochastic response of a hybrid energy harvesting system combining piezoelectric and electromagnetic technologies with viscoelastic materials, driven by narrowband colored noise. Especially, in bistable and multistable systems, SR phenomenon widely used in signal processing can be commonly observed.[41] Since the notion of SR was put forward, related researches have developed rapidly and been applied in many fields,[42–44] including mechanical fault detection.[45] Lei *et al.*[46] presented an underdamped SR method with steady-state matching to overcome the shortcomings of traditional SR method in weak feature extraction, which can diagnose early bearing faults. Li *et al.*[47] proposed a novel coupled bistable SR system, which made its output behavior have satisfactory bandpass filtering characteristic. Zhang and Lei[48] discussed the influence of Gaussian coloured noise on the logical SR of a cross-bifurcation nonsmooth system.

However, few studies consider simultaneously optimizing the performance of energy harvesting systems utilizing viscoelastic materials, time-delayed feedback control, and stochastic resonance. In addition, considering that all noises in nature have correlation time, which is colored noise. Therefore, the stochastic response and SR of viscoelastic bistable system with time-delayed feedback control driven by Gaussian colored noise and periodic excitation are analyzed in this paper.

The remaining parts of this paper are structured as follows: In Section 2, the model of bistable viscoelastic energy harvesting system controlled by time-delayed feedback is provided, and the equivalent system is obtained by stochastic averaging method of energy envelope. In Section 3, the steady-state probability density function (PDF) of equivalent system is obtained and the stochastic response of equivalent system is analyzed. In Section 4, the output signal-to-noise ratio (SNR) expression of the system is solved and then the SR analysis is proceeded. In Section 5, the conclusions of the paper are given.

2. System description and analysis

2.1. System governing equations

In the running automobile tires and other rotating machines, the vibration energy harvesting source of the energy harvesting system can be considered as the combination of random excitation and periodic excitation.[49] To improve the model, viscoelastic term is considered as damping term, and time-delayed feedback control of displacement and velocity is used. The energy harvester model with time-delayed feedback control coupled piezoelectric circuit operating in rotating environment is given Fig. 1, and its corresponding system governing equations are as follows:

$$\begin{aligned} &M\ddot{X}+Z+\frac{\mathrm{d}U_0(X)}{\mathrm{d}X}+k\bar{V}\\ &=-M\ddot{X}_{\mathrm{b}}+F(X_{\delta_1},\dot{X}_{\delta_2})+A_0G\sin(\Omega T),\\ &C_{\mathrm{p}}\dot{\bar{V}}+\frac{\bar{V}}{R}-k\dot{X}=0, \end{aligned} \tag{1}$$

where X and $\dot{X}$ are the relative displacement and velocity. Z and $\ddot{X}_\mathrm{b}$ represent the viscoelastic force and the base acceleration, respectively. $F(X_{\delta_1}, \dot{X}_{\delta_2}) = \Lambda_1 X(T-\delta_1) + \Lambda_2 \dot{X}(T-\delta_2)$ indicates the time-delayed feedback signal. $A_0 G\sin(\Omega T)$ is the harmonic excitation caused by the mass gravity G in a rotating environment, where A_0 and Ω denote the amplitude and frequency of this harmonic excitation, respectively. R, C_p, $\bar{V}$, k are the load resistance, the capacitance of the piezoelectric component, the voltage across resistance R, and the piezoelectric coupling coefficient, respectively. $U_0(X)$ denotes symmetric restoring force potential of mechanical oscillation system, which can be expressed as

$$U_0(X) = \frac{1}{2} r_1 (1-a) X^2 + \frac{1}{4} r_3 X^4, \tag{2}$$

where a, r_1, r_3 are tuning parameter, the linear and nonlinear spring constants, respectively. When nonlinear strength $r_3/r_1 > 0$ and tuning parameter $a > 1$, the system is nonlinear bistable with two stable equilibria at $X^*_{1,2} = \pm\sqrt{(a-1)/(r_3/r_1)}$, and the center $X^*_3 = 0$ is an unstable saddle point. Figure 2 shows the potential function $U_0(X)$ for different nonlinear strengths and tuning parameters.

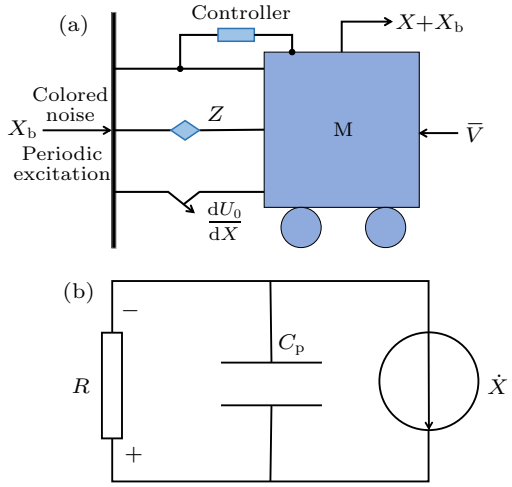


Fig. 1. A simplified structure for viscoelastic energy harvester controlled by time delay feedback: (a) mechanical diagram, (b) an equivalent circuit of piezoelectric mechanism.

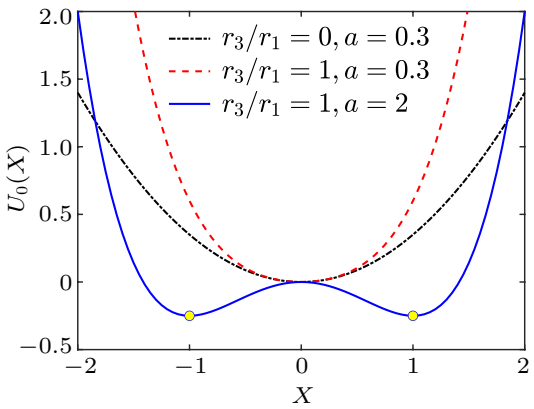


Fig. 2. Restoring force potential $U_0(X)$ for different nonlinear strengths and tuning parameters.

The following transformations are introduced to dimensionlessize the system equations:

$$\begin{aligned}
&x = X, \quad x_\mathrm{b} = X_\mathrm{b}, \quad \omega = \sqrt{\frac{r_1}{M}}, \quad t = \omega T, \quad \varsigma = \frac{1}{r_1},\\
&c_1 = a-1, \quad c_3 = \frac{r_3}{r_1}, \quad V = \frac{C_\mathrm{p}\bar{V}}{k},\\
&\theta = \frac{k^2}{r_1 C_\mathrm{p}}, \quad \mu = \frac{1}{C_\mathrm{p} R\omega}, \quad \lambda_1 = \frac{\Lambda_1}{r_1}, \quad \lambda_2 = \frac{\Lambda_2}{M\omega},\\
&\varepsilon = \frac{A_0}{r_1}, \quad \tau_1 = \omega\delta_1, \quad \tau_2 = \omega\delta_2.
\end{aligned} \tag{3}$$

According to the transformation [Eq. (3)], the dimensionless system governing equation can be obtained as

$$\begin{aligned}
&\ddot{x} + \varsigma Z - c_1 x + c_3 x^3 + \theta V\\
&= -\ddot{x}_\mathrm{b} + \lambda_1 x_{\tau_1} + \lambda_2 \dot{x}_{\tau_2} + \varepsilon G\sin(\Omega t), &\text{(4a)}\\
&\dot{V} + \mu V - \dot{x} = 0, &\text{(4b)}
\end{aligned}$$

in which x and $\dot{x}$ denote the dimensionless displacement and velocity of the mass M. ς, c_1, and c_2 are the coefficient of viscoelastic force Z, linear and nonlinear stiffness coefficients, respectively. λ_1 and τ_1 denote the feedback gain and time delay of the dimensionless displacement, while λ_2 and τ_2 denote that of the dimensionless velocity. θ, μ, and ε are the electromechanical coupling coefficient, time constant ratio, and the dimensionless coefficient of harmonic excitation, respectively. $-\ddot{x}_\mathrm{b} = \xi(t)$ is colored noise, indicating random excitation and satisfying

$$E[\xi(t)] = 0, \quad R(\tau) = E[\xi(t)\xi(t+\tau)] = \frac{D}{c}\exp\left(-\frac{|\tau|}{c}\right), \tag{5}$$

where c and D represent the correlation time and intensity of $\xi(t)$, respectively.

In system (4), the expression of viscoelastic term Z is

$$Z[x(t)] = \int_0^t G(t-\tau)x(\tau)\,\mathrm{d}\tau = \int_0^t G(u)x(t-u)\,\mathrm{d}u, \tag{6}$$

where $G(t)$ is the relaxation function that can be deduced from the generalized Maxwell model[50]

$$G(t) = \sum_i \beta_i \exp(-t/\alpha_i), \tag{7}$$

where α_i is the relaxation time of the viscoelastic force, which is non-negative. β_i denotes the magnitude of the viscoelastic force, which can be positive or negative.[51]

Substituting Eq. (7) into Eq. (6), Z can be rewritten as

$$Z = \int_0^t \sum_i \beta_i \exp(-s/\alpha_i)\, x(t-s)\,\mathrm{d}s. \tag{8}$$

2.2. Stochastic averaging method of energy envelope and the equivalent system

The generalized harmonic function is introduced to assume that the displacement and velocity of the system are in the following forms:

$$\begin{aligned} x(t) &= A(H(t))\cos\phi(t) - x_i^*, \\ \dot{x}(t) &= -A(H(t))\omega(H(t))\sin\phi(t), \\ \phi(t) &= \omega(H(t))t + \varphi(t), \end{aligned} \tag{9}$$

where x_i^* can be rewritten as $x_{1,2}^* = \pm\sqrt{c_1/c_3}, x_3^* = 0$ according to transformation (3). $i = 1,2,3$ in turn denote three motions, which are vibrating in the right potential well, vibrating in the left potential well and jumping between two potential wells. $\omega(H)$ and $A(H)$ represent the energy-dependent frequency and amplitude, and they both have slow varying processes. Thus, we can approximate the time-delayed feedback control of displacement and velocity as

$$\begin{aligned} x_{\tau_1} = x(t-\tau_1) &\approx (x(t) - x_i^*)\cos(\omega(H(t))\tau_1) \\ &\quad - \frac{\dot{x}}{\omega(H(t))}\sin(\omega(H(t))\tau_1), \end{aligned} \tag{10a}$$

$$\begin{aligned} \dot{x}_{\tau_2} = \dot{x}(t-\tau_2) &\approx (x(t) - x_i^*)\,\omega(H(t))\sin(\omega(H(t))\tau_2) \\ &\quad - \dot{x}(t)\cos(\omega(H(t))\tau_2). \end{aligned} \tag{10b}$$

Substituting Eq. (10a) into Eq. (8) and noting that the exponential decay term e^{-s/α_i} can be neglected while system (4) is subjected to excitation for a long time. The derivation of Eq. (11) below shows that Z can be approximated as a combination of the equivalent damping and stiffness terms.

$$\begin{aligned} Z &= \int_0^t \sum_i \beta_i \mathrm{e}^{-s/\alpha_i}\left[(x - x_i^*)\cos(\omega(H)s) - \frac{\dot{x}}{\omega(H)}\sin(\omega(H)s)\right]\mathrm{d}s \\ &= \sum_i \left\{ \frac{\beta_i\alpha_i}{1+\alpha_i^2\omega(H)^2}(x - x_i^*) - \frac{\beta_i\alpha_i^2}{1+\alpha_i^2\omega(H)^2}\dot{x} \right. \\ &\quad + \left[\beta_i(x - x_i^*)(\omega(H)\alpha_i\sin\omega(H)t - \cos\omega(H)t) \right. \\ &\quad \left. \left. + \frac{\beta_i\dot{x}}{\omega(H)}(\omega(H)\alpha_i\cos\omega(H)t + \sin\omega(H)t)\right] \right. \\ &\quad \left. \times \frac{\alpha_i \mathrm{e}^{-t/\alpha_i}}{1+\alpha_i^2\omega(H)^2}\right\} \\ &\approx \sum_i \left(\frac{\beta_i\alpha_i}{1+\alpha_i^2\omega(H)^2}(x - x_i^*) - \frac{\beta_i\alpha_i^2}{1+\alpha_i^2\omega(H)^2}\dot{x}\right). \end{aligned} \tag{11}$$

Let $i = 1$, ςZ can be written as

$$\varsigma Z = \frac{\varsigma\beta_1\alpha_1}{1+\alpha_1^2\omega(H)^2}(x - x_i^*) - \frac{\varsigma\beta_1\alpha_1^2}{1+\alpha_1^2\omega(H)^2}\dot{x}. \tag{12}$$

Integrating Eq. (4b) according to Eqs. (9) and (10b), and neglecting the transient exponential decay term, the expression for the steady-state part of voltage is obtained as follows:

$$\begin{aligned} V(t) &= C\mathrm{e}^{-\mu t} + \int_0^t \mathrm{e}^{-\mu(t-s)}\dot{x}\,\mathrm{d}s \approx \int_0^t \mathrm{e}^{-\mu\tau}\dot{x}(t-\tau)\,\mathrm{d}\tau \\ &\approx \frac{\omega^2(H(t))}{\mu^2+\omega^2(H(t))}(x(t) - x_i^*) \\ &\quad + \frac{\mu}{\mu^2+\omega^2(H(t))}\dot{x}(t). \end{aligned} \tag{13}$$

Substituting Eqs. (10), (12), and (13) into Eq. (4a), the expression for the equivalent decoupled system is obtained as

$$\ddot{x} + \tilde{\xi}\dot{x} - c_1 x + c_3 x^3 + \tilde{c}(x - x_i^*) = \xi(t) + \varepsilon G\sin(\Omega t), \tag{14}$$

in which

$$\begin{aligned} \tilde{\xi} &= -\frac{\varsigma\beta_1\alpha_1^2}{1+\alpha_1^2\omega(H)^2} + \frac{\theta\mu}{\mu^2+\omega^2(H)} \\ &\quad + \lambda_1\frac{\sin(\omega(H)\tau_1)}{\omega(H)} - \lambda_2\cos(\omega(H)\tau_2), \\ \tilde{c} &= \frac{\varsigma\beta_1\alpha_1}{1+\alpha_1^2\omega(H)^2} + \frac{\theta\omega^2(H)}{\mu^2+\omega^2(H)} \\ &\quad - \lambda_1\cos(\omega(H)\tau_1) - \lambda_2\omega(H)\sin(\omega(H)\tau_2). \end{aligned} \tag{15}$$

According to Eq. (14), the expressions for the potential function $U(x)$ and the total energy H can be obtained as follows:

$$\begin{aligned} U(x) &= \frac{1}{2}(\tilde{c} - c_1)x^2 + \frac{1}{4}c_3x^4, \\ H &= \frac{1}{2}\dot{x}^2 + \frac{1}{2}(\tilde{c} - c_1)x^2 + \frac{1}{4}c_3x^4. \end{aligned} \tag{16a}$$

Further analysis of the equivalent decoupled system Eq. (14) requires the energy-dependent frequency $\omega(H)$ to be obtained in advance, which in turn requires first obtaining the energy-dependent period $T(H)$. Due to the symmetry, the period expressions for the periodic motion of the left and right potential wells are the same and can both be expressed as

$$T(H) = 2\int_{x_{\min}}^{x_{\max}} \frac{\mathrm{d}x}{\sqrt{2H - 2U(x)}}, \tag{17}$$

where $x_{\max}$ and $x_{\min}$ represent the maximum and minimum displacements determined by $H = U(A)$ without time-delayed feedback control, respectively, which are expressed as follows:

$$\begin{aligned} x_{\max} &= \sqrt{\left(c_1 - \tilde{c}_0 + \sqrt{(c_1 - \tilde{c}_0)^2 + 4c_3H}\right)/c_3}, \\ x_{\min} &= \sqrt{\left(c_1 - \tilde{c}_0 - \sqrt{(c_1 - \tilde{c}_0)^2 + 4c_3H}\right)/c_3}, \end{aligned} \tag{18}$$

in which

$$\tilde{c}_0 = \frac{\varsigma\beta_1\alpha_1}{1+\alpha_1^2\omega(H)^2} + \frac{\theta\omega^2(H)}{\mu^2+\omega^2(H)}.$$

Furthermore, due to symmetry, $x_{\min} = -x_{\max}$ holds when the periodic motion is jumping between potential wells, and the period in this case can be expressed as

$$T(H) = 4\int_0^{x_{\max}} \frac{\mathrm{d}x}{\sqrt{2H - 2U(x)}}. \tag{19}$$

According to the relationship between $\omega(H)$ and $T(H)$ characterized by Eq. (20), $\omega(H)$ can be calculated by adopting the iterative algorithm.[52]

$$\omega(H) = \frac{2\pi}{T(H)}. \tag{20}$$

The total energy H and the energy-dependent frequency $\omega(H)$ of the bistable system without time-delayed feedback control are depicted Fig. 3. We can observe that when $H < 0$, i.e., the periodic motion being performed by the system is vibrating in the left or right potential well, $\omega(H)$ has two symmetric maxima at the two stable points and the rate of $\omega(H)$ decrease gradually increases as one moves away from the stable points. When $H > 0$, i.e., the periodic motion is jumping between potential wells, $\omega(H)$ increases rapidly with the increase of H.

Figure 4 depicts the variation of potential function $U(x)$ and potential well depth ΔU for various time-delayed feedback control parameters. The relationship between $U(X)$ and ΔU is given by $\Delta U = |\min(U(X))|$. As explained earlier in Eq. (2) for the parameter taking of the potential energy function, the system should be nonlinear and bistable when both parameters c_1 and c_3 are taken to be greater than 0. This is verified Figs. 4(a) and 4(b), which shows $U(x)$ as a displacement-dependent symmetric double-well potential function. Figure 4(a) also reveals that the increase of τ_2 leads to a periodic variation of $U(x)$. Figure 4(b) shows that varying the feedback gains of x and $\dot{x}$ can modify both well depth and well interval for two fixed time delays. Figures 4(a) and 4(b) reveal that the influence of increasing or decreasing the feedback gain λ_2 on the well depth ΔU varies with different values of time delay for either displacement or velocity time lag feedback control. The influence of the feedback gain on the potential energy function can only be determined when the time delay value is fixed.

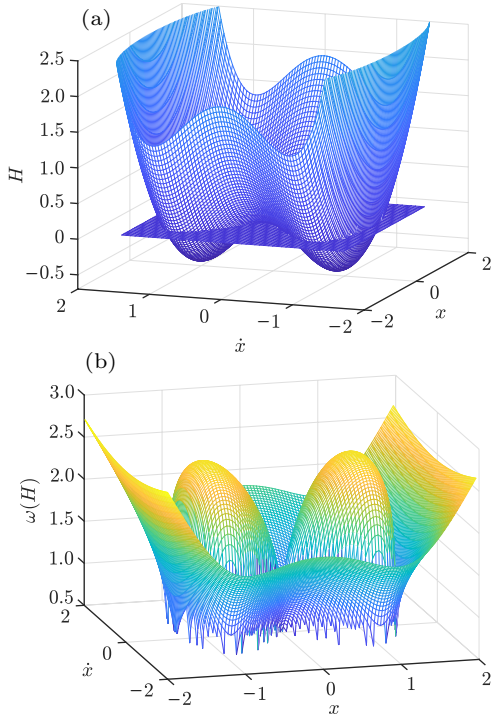


Fig. 3. (a) The total energy H and (b) the energy-dependent frequency $\omega(H)$ with fixed $c_1 = 3$, $c_3 = 3$, $\varsigma = 1$, $\beta_1 = -0.1$, $\alpha_1 = 1$, $\theta = 0.3$, $\mu = 0.05$.

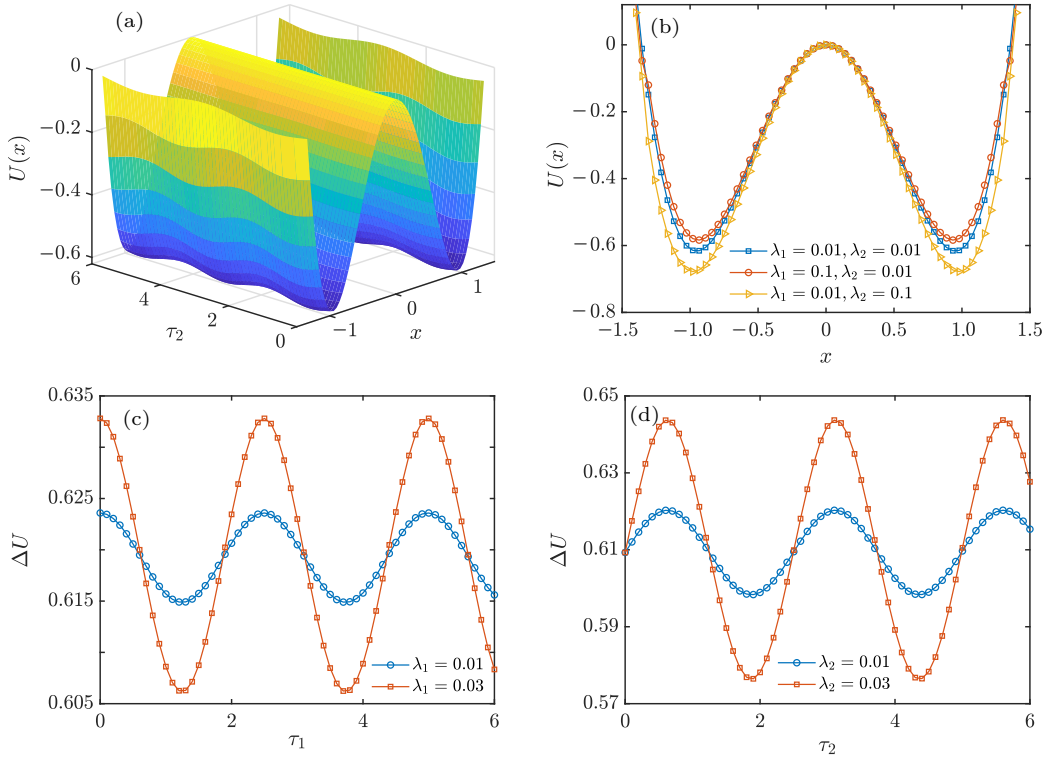


Fig. 4. Fixed system parameters $c_1 = 3$, $c_3 = 3$, $\varsigma = 1$, $\beta_1 = -0.1$, $\alpha_1 = 1$, $\theta = 0.3$, $\mu = 0.05$. (a) The potential $U(x)$ with fixed $\lambda_1 = 0.01$, $\lambda_2 = 0.01$, $\tau_1 = 1$. (b) The potential $U(x)$ for different (λ_1, λ_2) with fixed $\tau_1 = 1$, $\tau_2 = 1$. Panels (c) and (d) indicate the potential well depth ΔU in respect to τ_1 and τ_2, respectively, with fixed $(\lambda_2, \tau_2) = (0.01, 1)$ and $(\lambda_1, \tau_1) = (0.01, 1)$ in turn.

3. Stochastic response

After subtracting Eq. (16a) from Eq. (16b) and performing simultaneous open square operations on the left and right sides of the resulting new equation, the velocity of the system expressed in terms of potential $U(x)$ and total energy H can be obtained

$$\dot{x} = \sqrt{2H - 2U(x)}. \tag{21}$$

The first derivative of the total energy H can be obtained by taking the derivative of t on both sides of Eq. (16b)

$$\dot{H} = -\dot{x}\left[\ddot{x} + (\tilde{c} - c_1)x + c_3x^3\right]. \tag{22}$$

Transforming Eq. (14) to obtain the expression for $\ddot{x}$, substituting it into the above equation. Then, the equivalent decoupled system Eq. (14) can be expressed as two first-order equations for the system velocity $\dot{x}$ and the total energy H, as follows:

$$\begin{aligned} &\dot{x} = \sqrt{2H - 2U(x)}, \\ &\dot{H} = -\dot{x}(\tilde{\varsigma}\dot{x} - \tilde{c}x_i^*) + \dot{x}\xi(t) + \dot{x}\varepsilon G\sin(\Omega t). \end{aligned} \tag{23}$$

Since the energy process $H(t)$ can be approximated as a Markov diffusion process, the stochastic averaging method of the energy envelope can be applied to obtain the average Itô equation governing $H(t)$ as follows:

$$\mathrm{d}H = m(H)\,\mathrm{d}t + \sigma(H)\,\mathrm{d}B(t), \tag{24}$$

where $m(H)$, $\sigma(H)$, $B(t)$ denote the drift coefficient, diffusion coefficient, and standard Wiener process, respectively. $m(H)$ and $\sigma(H)$ can be expressed as follows:

$$\begin{aligned} m(H) &= -\left\langle \dot{x}(\tilde{\varsigma}\dot{x} - \tilde{c}x_i^*)\right\rangle_t + \frac{D}{1 + c^2\omega^2(H)} + \left\langle \dot{x}\varepsilon G\sin(\Omega t)\right\rangle_t, \\ \sigma^2(H) &= \frac{2D}{1 + c^2\omega^2(H)}\left\langle \dot{x}^2\right\rangle_t, \end{aligned} \tag{25}$$

where $\langle(\cdot)\rangle_t = \frac{1}{T}\int_0^T(\cdot)\,\mathrm{d}t$ represents the time averaging calculation. Meanwhile, in the absence of harmonic excitation, according to the symmetry of the left and right potential wells, we can obtain

$$\begin{aligned} \left\langle \dot{x}x_i^*\right\rangle_t &= \frac{1}{T}\int_0^T \dot{x}x_i^*\,\mathrm{d}t = \frac{1}{T}\oint x_i^*\,\mathrm{d}x \\ &= \frac{1}{T_r + T_l}\left[\oint_r x_1^*\,\mathrm{d}x + \oint_l x_2^*\,\mathrm{d}x\right]. \end{aligned} \tag{26}$$

Then, according to the Itô equation (24), the steady-state PDF of the total energy $p(H)$ can be obtained

$$p(H) = \frac{N^{-1}}{\sigma^2(H)}\exp\left(\int \frac{2m(H)}{\sigma^2(H)}\,\mathrm{d}H\right), \tag{27}$$

in which N^{-1} denotes a normalization constant.

Therefore, according to $(\mathrm{d}/\mathrm{d}H)\ln\left[T(H)\langle\dot{x}^2\rangle_t\right] = \langle\dot{x}^2\rangle_t^{-1}$,[53] the joint steady-state PDF of the equivalent system Eq. (14) can be obtained by the following derivation:

$$\begin{aligned} p(x,\dot{x}) &= \frac{p(H)}{T(H)} = \frac{N^{-1}\langle\dot{x}^2\rangle_t}{\sigma^2(H)} \\ &\quad\times\exp\left[\int_0^H\left(\frac{2m(s)}{\sigma^2(s)} - \frac{1}{\langle\dot{x}^2\rangle_t}\right)\mathrm{d}s\right] \\ &= \frac{N^{-1}(1 + c^2\omega^2(H))}{D} \\ &\quad\times\exp\left[\frac{-\tilde{\varsigma}(1 + c^2\omega^2(H))}{D}\left(\frac{1}{2}\dot{x}^2 + \frac{1}{2}(\tilde{c} - c_1)x^2\right.\right. \\ &\quad\left.\left. + \frac{1}{4}c_3x^4 - x\varepsilon G\sin(\Omega t)\right)\right]. \end{aligned} \tag{28}$$

Further, the expressions for the mean square voltage $E\left[V^2\right]$ and mean output power $E[P]$ can be derived from Eq. (13) and (28) as follows:

$$\begin{aligned} E\left[V^2\right] &= \int_{-\infty}^{\infty}\int_{-\infty}^{\infty}\left(\frac{\omega^2(H)}{\mu^2 + \omega^2(H)}(x - x_i^*)\right. \\ &\quad\left. + \frac{\mu}{\mu^2 + \omega^2(H)}\dot{x}\right)p(x,\dot{x})\,\mathrm{d}x\mathrm{d}\dot{x}, \\ E[P] &= \theta\mu E\left[V^2\right]. \end{aligned} \tag{29}$$

$p(x,\dot{x})$, $E[V^2]$, and $E[P]$ obtained by the stochastic averaging method of the energy envelope, are important indicators to characterize the performance of the vibration energy harvester. Therefore, it is necessary to verify the accuracy of the adopted theoretical analysis method, which can be done by comparing the agreement between the numerical results obtained from the Monte Carlo method and the analytical results obtained from the adopted theoretical method.

Meanwhile, the previous analysis Fig. 4 regarding the effect of the time-delayed feedback control parameters on the potential function in the absence of harmonic excitation reveals that the time-delayed feedback control may have an important impact on the performance of the vibration energy harvesting system. Therefore, the impact of time-delayed feedback control on mean output power $E[P]$ under harmonic-free excitation will be analyzed accordingly in this section. In addition, since viscoelastic damping is considered, the effect of viscoelastic parameters on the system performance will also be discussed. An example is given here and the main parameters of the system are fixed as $c_1 = 3$, $c_3 = 3$, $\theta = 0.3$, $\mu = 0.05$, $\varsigma = 1$, $\beta_1 = -0.1$, $\alpha_1 = 1$, $D = 0.004$, $c = 0.3$ in the absence of other mentions.

Figures 5 and 6 show the theoretical and numerical results obtained by the stochastic averaging method of energy envelope and the Monte Carlo method, respectively. The results exhibit a high level of agreement. Figure 5 shows the joint probability density function, while figure 6 shows the marginal probability density function. The theoretical and numerical results are represented by the solid line and circle symbols in Fig. 6.

The comparison of Figs. 6(a) and 6(b) reveals that the increase in noise intensity D increases $p(x)|_{x=0}$, which reveals that the transition between two potential wells occurs relatively easily. In contrast, the comparison of Figs. 6(a) and 6(c) shows that the increase in the correlation time c makes the peak value of $p(x)$ larger, which means that the transition between the two potential wells is relatively difficult. In addition, it can be noticed from Fig. 6(d) that the increase in noise intensity broadens the range of the SR, while the correlation time has little effect.

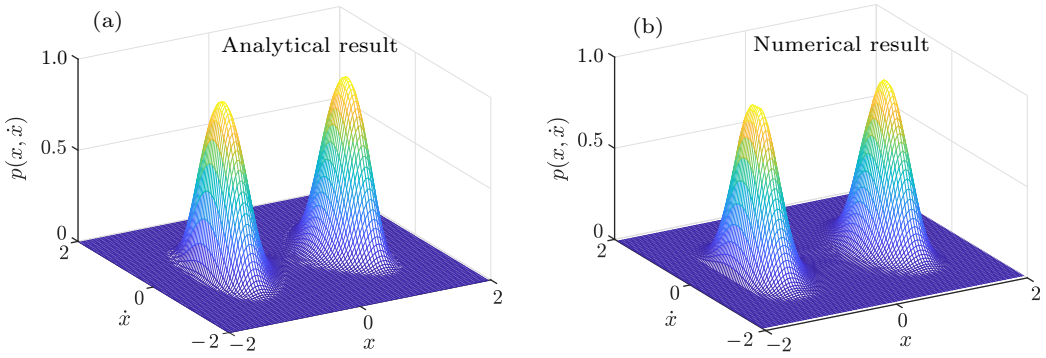


Fig. 5. Comparisons between analytical results (a) and numerical results (b) of joint stationary PDF with fixed $\lambda_1 = 0.01$, $\lambda_2 = 0.01$, $\tau_1 = 1.5$, $\tau_2 = 1.5$.

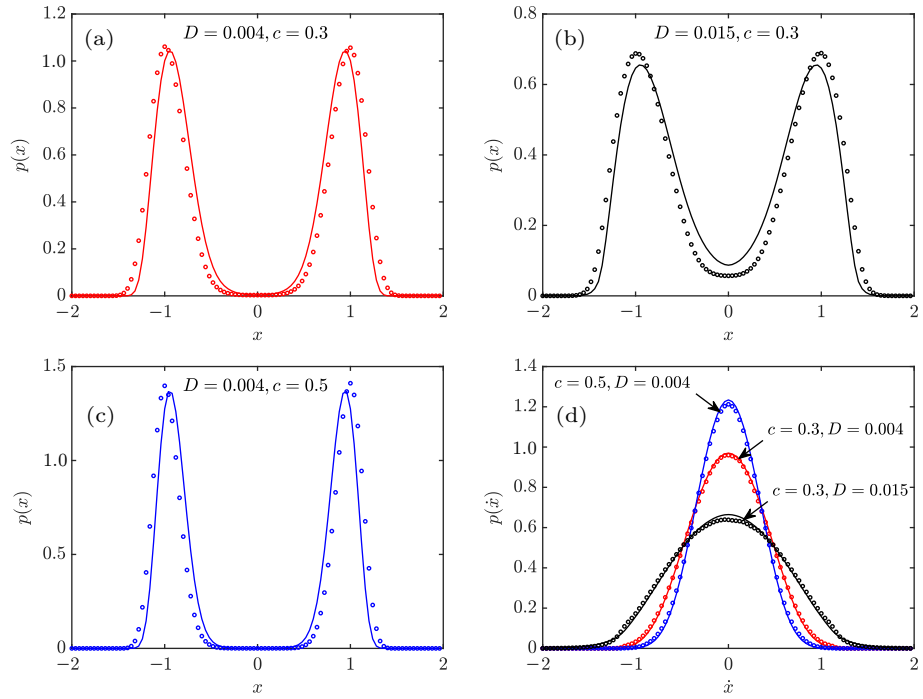


Fig. 6. Comparisons of stationary PDF of displacement x and velocity $\dot{x}$ for different D and c, with fixed $\lambda_1 = 0.01$, $\lambda_2 = 0.01$, $\tau_1 = 1.5$, $\tau_2 = 1.5$.

The dependence of the mean output power $E[P]$ on the time delay is depicted Fig. 7. Figure 7(a) shows that the unidirectional variation of either the time delay τ_1 of the displacement or the time delay τ_2 of the velocity results in a consequent periodic variation of $E[P]$. Thereby, $E[P]$ has many local peaks that can be reached by choosing the corresponding time delay combination (τ_1, τ_2) in the region of concern. For example, in the region $S = \{(\tau_1, \tau_2)|\tau_1 \in [0,2], \tau_2 \in [2,4]\}$, the peak of $E[P]$ on the region S is obtained at the point of the time delay combination $(\tau_1, \tau_2) = (0.6, 2.4)$ labeled Fig. 7(a). It can be observed Fig. 7(b) that under the same displacement delay feedback control, the output performance of system that also considers velocity delay feedback at $(\lambda_2, \tau_2) = (0.005, 2.4)$ is significantly better than one of the displacement delay feedback control only. Figure 7(b) also reveals that the effect of the displacement feedback gain λ_1 on the output power $E[P]$ is similar to its effect on the well depth ΔU, i.e., both need to be at a determined value of the time delay to discuss whether the effect of increasing λ_1 brings a positive or negative effect on $E[P]$.

It can be observed Fig. 7(b) that the effect of the feedback gain on the output power at smaller time delays is opposite to that at larger time delays in the time delay range of $[0,2]$, and the case at smaller time delays can be inferred by obtaining the case at larger time delays. Figure 8(a) depicts the variation of mean output power $E[P]$ with the displacement

feedback gain λ_1 and velocity feedback gain λ_2 for time delay $(\tau_1, \tau_2) = (1.5, 1.5)$. The results show that $E[P]$ increases with λ_1 and decreases with λ_2, i.e., taking a combination of larger displacement positive feedback gain and velocity negative feedback gain is more effective in increasing $E[P]$.

Thus, a larger combination of positive feedback gain and negative feedback gain$(\lambda_1, \lambda_2) = (0.01, -0.01)$ with $(\tau_1, \tau_2) = (1.5, 1.5)$ under control is observed in Figs. 8(b), 8(d), 9, and 10 compared with the uncontrolled case. Obviously, figure 8 shows the output power in the control case is better than that in the uncontrolled case for different noise intensities and viscoelastic parameters. However, after the magnitude of viscoelastic force β_1 reaches a certain value, control or not has no effect on the output power. According to Figs. 8(c) and 8(d), it is suggested to adopt a smaller α_1 and a relatively larger β_1, which can achieve a greater mean output power $E[P]$ and better system performance. The results of Fig. 8 show that improving the performance of the time-delayed feedback-controlled energy harvester can be achieved by selecting appropriate time-delayed control parameters.

Figure 9 shows the influence of linear stiffness coefficient c_1 and nonlinear stiffness coefficient c_3 on mean output power $E[P]$. It can be observed in Fig. 9 that $E[P]$ first increases and then decreases with the increase of c_1, which means that there is an optimum value of c_1 around 0.8 to maximise $E[P]$, while the change of $E[P]$ caused by the increase of c_3 is just the opposite, first decreasing and then increasing. Meanwhile, figure 9 reveals that when the stiffness coefficients c_1 and c_3 are large, $E[P]$ under the considered time-delayed feedback control is larger than that without the time-delayed feedback control. Therefore, the energy harvester can improve its performance by adopting appropriate stiffness coefficients, such as $c_1 = 0.8$ and smaller c_3.

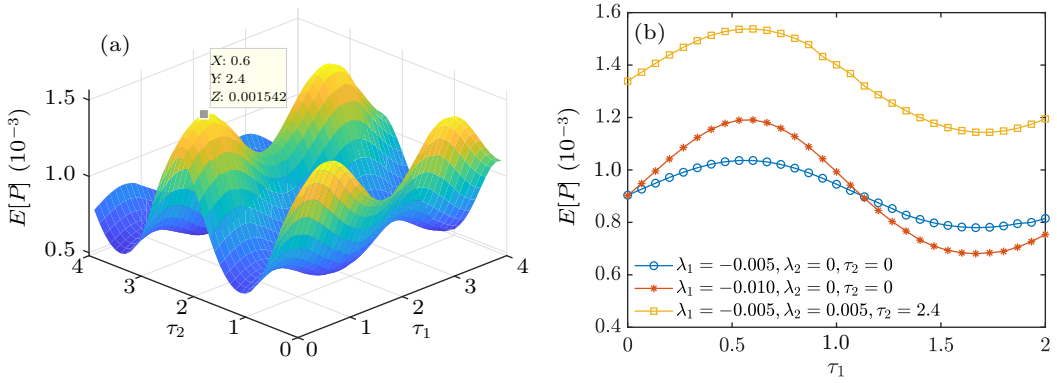


Fig. 7. (a) The mean output power $E[P]$ regarding τ_1 and τ_2 with fixed $\lambda_1 = -0.005$, $\lambda_2 = 0.005$. (b) The mean output power $E[P]$ regarding τ_1 for different time-delayed feedback control parameters $(\lambda_1, \lambda_2, \tau_2)$.

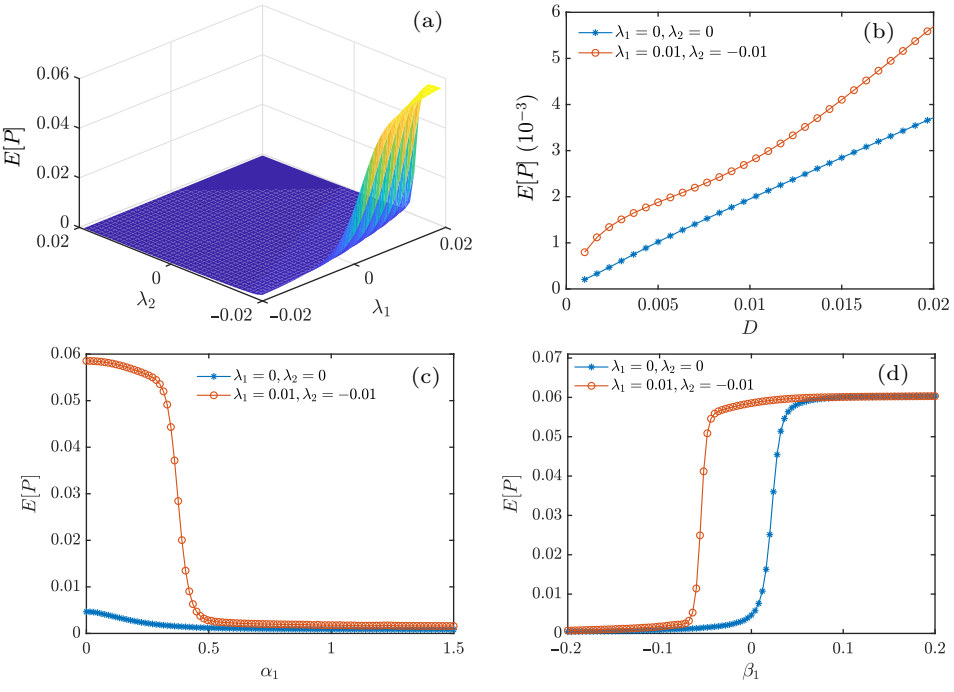


Fig. 8. Fixed time delays $(\tau_1, \tau_2) = (1.5, 1.5)$. (a) The mean output power $E[P]$ regarding λ_1 and λ_2. (b) The mean output power $E[P]$ regarding D for different (λ_1, λ_2). (c) The mean output power $E[P]$ regarding α_1 for different (λ_1, λ_2). (d) The mean output power $E[P]$ regarding β_1 for different (λ_1, λ_2).

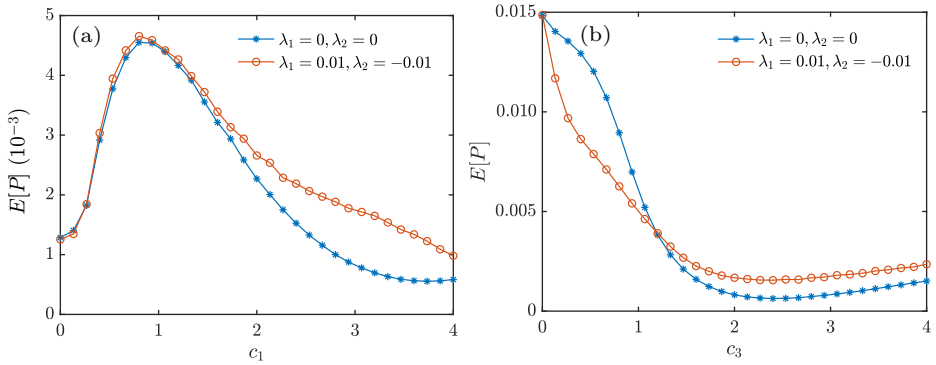


Fig. 9. (a) The mean output power $E[P]$ regarding c_1 for different (λ_1, λ_2). (b) The mean output power $E[P]$ regarding c_3 for different (λ_1, λ_2).

Figure 10 illustrates the dependence of mean output power $E[P]$ on electromechanical coupling coefficient θ and time constant ratio μ. In Fig. 10, the increase of θ and μ both cause the increase of $E[P]$. The difference is that with the increase of θ, the growth rate of $E[P]$ also increases, while the rate of $E[P]$ increase caused by the increase of μ gradually slows down. According to the analysis of Fig. 10, larger θ and μ are beneficial to improve the system performance.

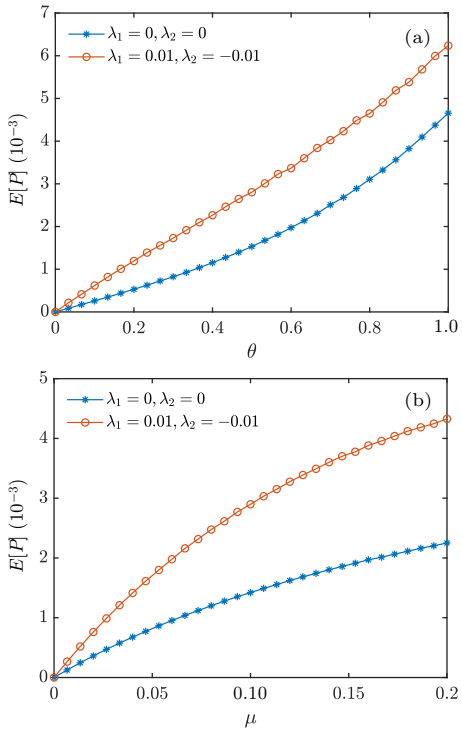


Fig. 10. (a) The mean output power $E[P]$ regarding θ for different (λ_1, λ_2). (b) The mean output power $E[P]$ regarding μ for different (λ_1, λ_2).

Figures 7–10 demonstrate that the system output performance can be effectively improved by using appropriate time-delayed feedback control parameters.

4. Stochastic resonance

The response analysis of the system shows that the time-delayed feedback control without harmonic excitation has a significant effect on the system performance improvement. Meanwhile, in order to harvest as much electrical energy as possible in the external environment, the time-delayed feedback control energy harvester is mounted on the vehicle tires to achieve uniform excitation of the energy harvester through the periodic excitation caused by the gravity of the object while the vehicle is operating, which has been verified to effectively improve the energy harvesting efficiency of the system.[49,54] Existing theoretical studies clearly reveal that the system can generate large amplitude vibrations in the presence of SR phenomena.[19,55] It is noted that the SNR serves as an important indicator for determining the SR of the system, revealing the SR phenomenon of the system when the peak occurs. Therefore, in this section, SR is applied to optimize the energy harvesting efficiency and characterize the effect of different parameters on the system performance under time-delayed feedback control by observing the effect of each parameter on the theoretical output SNR.

The governing equation of the vibration energy harvesting system Eq. (14) subjected to simultaneous excitation by harmonics and random noise can be equivalently written as

$$\begin{aligned} \dot{x} &= y, \\ \dot{y} &= \tilde{\xi} y + c_1 x - c_3 x^3 - \tilde{c}(x - x_i^*) + \xi(t) + \varepsilon G \sin(\Omega t). \end{aligned} \tag{30}$$

According to the stationary PDF derived Eq. (28), the effective generalized potential functions of the system displacement and velocity U_{e} can be expressed as follows:[56]

$$\begin{aligned} U_{\mathrm{e}}(x, \dot{x}, t) = \tilde{\xi}(1 + c^2 \omega^2(H)) \Big(& \frac{1}{2}\dot{x}^2 + \frac{1}{2}(\tilde{c} - c_1)x^2 \\ & + \frac{1}{4} c_3 x^4 - x \varepsilon G \sin(\Omega t) \Big). \end{aligned} \tag{31}$$

Let $(x, \dot{x}) = (0, 0)$, solving the deterministic model of system Eq. (30) without external excitation and time-delayed feedback control, the following two stationary equilibrium points $(x_{s_1, s_2}, 0)$ and one non-stationary equilibrium point $(x_u, 0)$ can be obtained

$$\begin{aligned} x_{s_1} &= \sqrt{(c_1 - \tilde{c}_0)/c_3}, \\ x_{s_2} &= -\sqrt{(c_1 - \tilde{c}_0)/c_3}, \quad x_u = 0. \end{aligned} \tag{32}$$

Linearize Eq. (30) at equilibrium points $(x_{s_1},0),(x_{s_2},0)$ and $(x_u,0)$, and solve the corresponding characteristic equations to obtain their eigenvalues, as follows:

$$\begin{aligned}\lambda_{s_1,s_2}^{\pm} &= \frac{1}{2}\left[-\tilde{\varsigma}_0 \pm \sqrt{|\tilde{\varsigma}_0{}^2 - 8\,(c_1-\tilde{c}_0)\,|}\right],\\ \lambda_u^{\pm} &= \frac{1}{2}\left[-\tilde{\varsigma}_0 \pm \sqrt{\tilde{\varsigma}_0{}^2 + 4\,(c_1-\tilde{c}_0)}\right],\end{aligned} \tag{33}$$

where

$$\tilde{\varsigma}_0 = -\frac{\varsigma\beta_1\alpha_1^2}{1+\alpha_1^2\omega(H)^2} + \frac{\theta\mu}{\mu^2+\omega^2(H)}.$$

Using the steepest descent method[57,58] and based on the definition of the mean first passage time, the mean first passage time of a particle from one stable point to another can be deduced as

$$T_{\rm fp} = 2\pi\sqrt{\frac{\lambda_u^-}{\lambda_{s_i}^+\lambda_{s_i}^-\lambda_u^+}}\exp\left[\frac{U_{\rm e}(x_u,0,t)-U_{\rm e}(x_{s_i},0,t)}{D}\right]. \tag{34}$$

Thereby, we can obtain the expressions for the transition rates $W_{1,2}$ of the particles escaping from the potential wells where x_{s_1} and x_{s_2} are located, respectively, as follows:

$$W_i = \frac{1}{2\pi}\sqrt{\frac{\lambda_{s_i}^+\lambda_{s_i}^-\lambda_u^+}{\lambda_u^-}}\exp\left[\frac{U_{\rm e}(x_{s_i},0,t)-U_{\rm e}(x_u,0,t)}{D}\right]. \tag{35}$$

Substituting $U_{\rm e}$ expressed by Eq. (31) into Eq. (35), the transition rate W_i can be formulated as

$$\begin{aligned}W_i &= \frac{1}{2\pi}\sqrt{\frac{\lambda_{s_i}^+\lambda_{s_i}^-\lambda_u^+}{\lambda_u^-}}\exp\left[\frac{\tilde{\varsigma}(1+c^2\omega^2(H))}{D}\right.\\ &\quad\times\left(\frac{1}{2}\dot{x}_{s_i}^2+\frac{1}{2}(\tilde{c}-c_1)x_{s_i}^2\right.\\ &\quad\left.\left.+\frac{1}{4}c_3x_{s_i}^4-x_{s_i}\varepsilon G\sin(\Omega t)\right)\right].\end{aligned} \tag{36}$$

Performing a Taylor expansion on the $-x_{s_i}\varepsilon G\sin(\Omega t)$ term of the exponent Eq. (36), the transition rate W_i can be approximated as

$$\begin{aligned}W_i &= w_0\left[1-\frac{\tilde{\varsigma}(1+c^2\omega^2(H))}{D}x_{s_i}\varepsilon G\sin(\Omega t)+\cdots\right]\\ &\approx w_0+w_1\varepsilon G\sin(\Omega t),\end{aligned} \tag{37}$$

in which

$$\begin{aligned}w_0 &= \frac{1}{2\pi}\sqrt{\frac{\lambda_{s_i}^+\lambda_{s_i}^-\lambda_u^+}{\lambda_u^-}}\exp\left[\frac{\tilde{\varsigma}(1+c^2\omega^2(H))}{D}\right.\\ &\quad\times\left.\left(\frac{1}{2}\dot{x}_{s_i}^2+\frac{1}{2}(\tilde{c}-c_1)x_{s_i}^2+\frac{1}{4}c_3x_{s_i}^4\right)\right],\\ w_1 &= -w_0\frac{\tilde{\varsigma}(1+c^2\omega^2(H))}{D}x_{s_i}.\end{aligned} \tag{38}$$

Then, the signal output power spectrum $S_1(\Omega_{\rm d})$ and the noise output power spectrum $S_2(\Omega_{\rm d})$ can be obtained separately as follows:

$$\begin{aligned}S_1(\Omega_{\rm d}) &= \frac{\pi x_{s_i}^2w_1^2\varepsilon^2G^2}{2(w_0^2+\Omega^2)}\left[\delta(\Omega_{\rm d}-\Omega)+\delta(\Omega_{\rm d}+\Omega)\right],\\ S_2(\Omega_{\rm d}) &= \left[1-\frac{w_1^2\varepsilon^2G^2}{2(w_0^2+\Omega^2)}\right]\frac{2x_{s_i}^2w_0}{w_0^2+\Omega_{\rm d}^2}.\end{aligned} \tag{39}$$

Therefore, according to the definition of SNR, its expression can be derived as follows:

$$\begin{aligned}{\rm SNR} &= \frac{\int_0^\infty S_1(\Omega_{\rm d})\,{\rm d}\Omega_{\rm d}}{S_2(\Omega_{\rm d}=\Omega)}\\ &= \frac{\pi w_1^2\varepsilon^2G^2}{4w_0}\left[1-\frac{w_1^2\varepsilon^2G^2}{2(w_0^2+\Omega^2)}\right]^{-1}.\end{aligned} \tag{40}$$

Figures 11 and 12 depict the effect of the time-delayed feedback control parameters on the output SNR as a function of the noise intensity D. The results show that the optimal noise intensity D exists for different parameters to maximize the output SNR, which indicates the appearance of SR phenomena. In addition, the increase or decrease of the maximum value of the output SNR corresponds to the strengthening and weakening of the SR phenomenon, respectively.

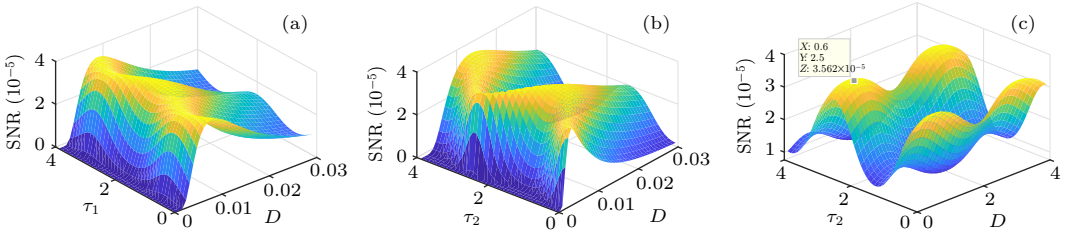


Fig. 11. (a) SNR regarding D and τ_1 with fixed $\lambda_1=-0.01$ in absence of time-delayed feedback control of $\dot{x}$; (b) SNR regarding D and τ_2 with fixed $\lambda_2=0.01$ in absence of time-delayed feedback control of x; (c) SNR regarding τ_1 and τ_2 with fixed $(\lambda_1,\lambda_2)=(-0.005,0.005)$.

Figure 11 depicts the variation of SNR with respect to the time delay. The results of Figs. 11(a) and 11(b) show that the effect of time delays τ_1 and τ_2 on SNR is non-monotonic and periodic within the noise intensity range considered. This reveals that perhaps the SNR can be driven to peak in the region of interest by selecting the proper combination of time delays (τ_1,τ_2), which is verified Fig. 11(c). The joint graph of SNR with respect to time delays τ_1 and τ_2 presents multiple peaks, and several combinations of time delays (τ_1,τ_2) for which the SNR peaks are obtained presumably coincide with the combi-

nations of time delays for which the $E[P]$ peaks are reached as depicted Fig. 7(a). For example, in region $S = \{(\tau_1, \tau_2)|\tau_1 \in [0,2], \tau_2 \in [2,4]\}$, $E[P]$ peaks at $(\tau_1, \tau_2) = (0.6, 2.4)$, while SNR achieves its peak at $(\tau_1, \tau_2) = (0.6, 2.5)$. This indirectly verifies that the occurrence of random resonance phenomenon is beneficial to enhance the system performance.

Figure 12 depicts the effect of feedback gains λ_1 and λ_2 on SNR. Figure 12(a) shows that for a fixed displacement time delay $\tau_1 = 1.5$, the SNR increases first to a peak and then decreases with increasing noise intensity D for different values of displacement feedback gain λ_1. In addition, as λ_1 increases, the peak SNR increases and the noise intensity at the peak decreases. Figure 12(b) shows that for a fixed velocity delay $\tau_2 = 1.5$, the SNR increases and then decreases with decreasing velocity feedback gain λ_2 for small noise intensity, which indicates that the variation of λ_2 induces the SR phenomenon. Meanwhile, under weak noise excitation, it can be noticed that the velocity feedback gain is a larger negative feedback when the SR occurs. Therefore, with fixed time delay $(\tau_1, \tau_2) = (1.5, 1.5)$, the larger positive displacement feedback and negative velocity feedback are beneficial to the SR occurrence and improve the system output performance when the intensity of the random excitation is small.

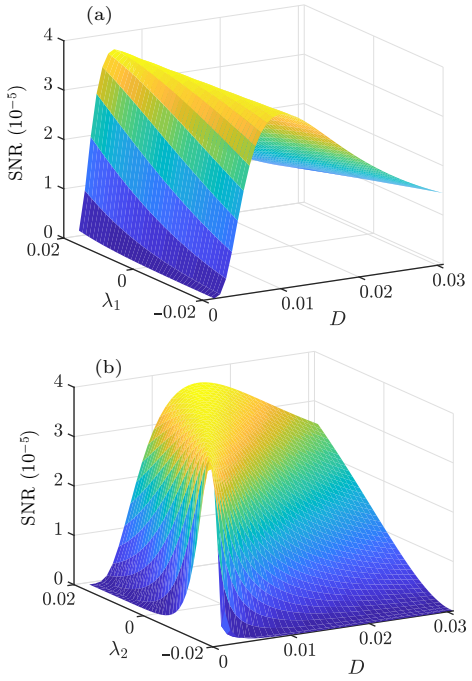


Fig. 12. (a) SNR regarding D and λ_1 with fixed $\tau_1 = 1.5$ in absence of time-delayed feedback control of $\dot{x}$; (b) SNR regarding D and λ_2 with fixed $\tau_2 = 1.5$ in absence of time-delayed feedback control of x.

Based on the previous conclusions on the effect of feedback gain on SR, figures 13–15 illustrate the variation of SNR affected by system parameters for larger combination of displacement positive feedback gain and velocity negative feedback gain $(\lambda_1, \lambda_2) = (0.01, -0.01)$ with time delay fixed at $(\tau_1, \tau_2) = (1.5, 1.5)$.

Figure 13 shows the SNR respect to D under multiple viscoelastic parameters α_1 and β_1, illustrating the influence of α_1 and β_1 on SNR. The results of Fig. 13 reveal that no SR occurs when α_1 is small or β_1 is relatively large. As α_1 increases and β_1 decreases, the peak value of SNR decreases and the excitation intensity required to reach the peak increases. This indicates that a less large α_1 and a relatively large β_1, for example $(\alpha_1, \beta_1) = (0.5, -0.1)$, can be chosen to enhance the system performance by the SR phenomenon.

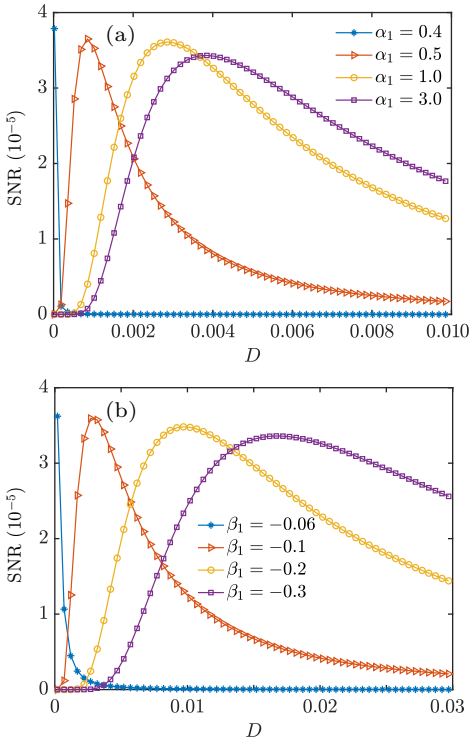


Fig. 13. SNR regarding D with fixed $\lambda_1 = 0.01$, $\lambda_2 = -0.01$, $\tau_1 = 1.5$, $\tau_2 = 1.5$: (a) for different α_1, (b) for different β_1.

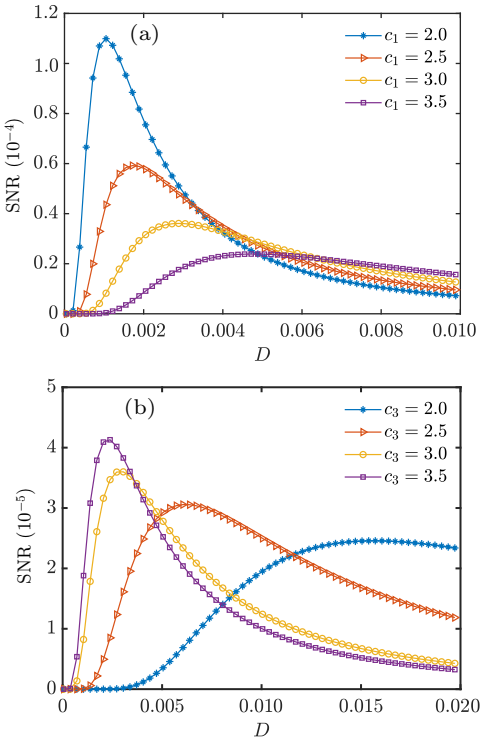


Fig. 14. SNR regarding D with fixed $\lambda_1 = 0.01$, $\lambda_2 = -0.01$, $\tau_1 = 1.5$, $\tau_2 = 1.5$: (a) for different c_1, (b) for different c_3.

Figure 14 depicts the linear stiffness coefficient c_1 and nonlinear stiffness coefficient c_3 impact on SNR. Figure 14 shows that the peak of SNR decrease with the increase of linear stiffness coefficient c_1 and the decrease of nonlinear stiffness coefficient c_3, which means that the intensity of SR phenomenon is weakened. Simultaneously, the noise intensity D required to reach the peak value increases, which indicates that the SR behavior needs greater random excitation. In addition, SNR is more sensitive to the change of linear stiffness coefficient c_1 than nonlinear stiffness coefficient c_3. The above results reveal that under weak noise excitation, the smaller linear stiffness coefficients c_1 and larger nonlinear stiffness coefficient c_3 is recommended to induce the SR phenomenon, and then improve the system performance.

The influence of electromechanical coupling coefficient θ and time constant ratio μ on SNR is depicted in Fig. 15. It can be observed in Fig. 15(a) that as θ increases, the peak value of SNR increases obviously, while the noise intensity D corresponding to the peak value increases slightly. Contrary to the influence of θ increase on SNR, figure 15(b) shows that with the increase of μ, the peak value of SNR decreases weakly and the noise intensity required to reach the peak value increases obviously. Therefore, choosing a larger electromechanical coupling coefficient θ and a smaller time constant ratio μ can conducive to the strong SR phenomenon to promote the system performance.

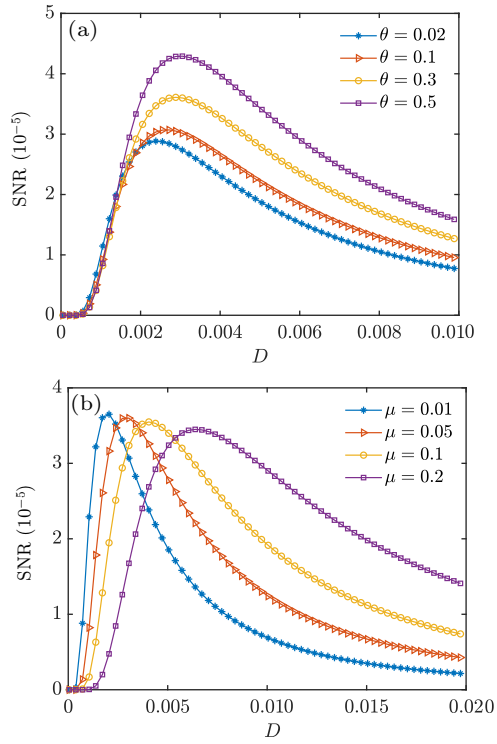


Fig. 15. SNR regarding D with fixed $\lambda_1 = 0.01$, $\lambda_2 = -0.01$, $\tau_1 = 1.5$, $\tau_2 = 1.5$: (a) for different θ, (b) for different μ.

Based on the conclusions in Section 3, the preferred time-delayed feedback control parameters for Figs. 11–15 are selected. The induction of stochastic resonance phenomena by the various system parameters under different noise intensities is analyzed, and the obtained results of the investigation and the conclusions in Section 3 can be roughly echoed.

5. Conclusions

In this paper, the stochastic response and stochastic resonance (SR) of a bistable energy harvesting system with viscoelastic material under colored noise excitation in a rotating environment were studied. Initially, the dimensionless governing equation of the system was derived, and the viscoelastic term was approximated as a combination of stiffness term and damping term by the stochastic averaging method of energy envelope, and then the equivalent system was derived by decoupling the system. Furthermore, the steady-state probability density function (PDF) of the equivalent system was deduced, and the effectiveness of adopted method was validated by contrasting the consistency between the numerical and the analytical results. The influence of time-delayed feedback control parameters and system parameters on mean output power was analyzed to give suggestions for improving system performance. In addition, the impact of various parameters on the SR behavior indicated by the signal-to-noise ratio (SNR) in the rotating environment was considered to further improve the system performance. Combined with the analyses of mean output power $E[P]$ and SNR under different parameters, the following suggestions can be given to improve the output performance of the system in rotating environment:

(i) The optimal performance of that system in the interest delay range can be achieved by choosing appropriate time delay groups (τ_1, τ_2).

(ii) Under weak noise excitation, fixed time delays $(\tau_1, \tau_2) = (1.5, 1.5)$, large positive displacement feedback and negative velocity feedback can induce strong random resonance and promote system performance.

(iii) As for the parameters of viscoelastic force, the smaller relaxation time α_1 and the larger magnitude β_1 can obtain larger $E[P]$ and SNR, which symbolizes the excellent output performance of system.

(iv) The influence of stiffness coefficients c_1 and c_3 on the system performance can be reflected in $E[P]$ and SNR. The results show that smaller linear stiffness coefficient and larger nonlinear stiffness coefficient can promote the system efficiency.

(v) Larger electromechanical coupling coefficient θ and smaller time constant μ are more conducive to the appearance of strong SR behavior, which means that these are recommended to increase the energy harvesting efficiency of the system.

Acknowledgements

Project supported by the National Natural Science Foundation of China (Grant No. 11902081), the Science and Tech-

nology Projects of Guangzhou (Grant No. 202201010326), and the Guangdong Provincial Basic and Applied Basic Research Foundation (Grant No. 2023A1515010833).

References

[1] Sun Y H, Zeng Y H and Yang Y G 2024 *Acta Mechanica Sinica* **40** 523154
[2] Tian Y, Lu X, Wang B, Tang B and Xu M 2023 *Journal of Vibration Engineering & Technologies* 1–10
[3] Pfenniger A, Wickramarathna L N, Vogel R and Koch V M 2013 *Medical Engineering & Physics* **35** 1256
[4] Fezeu G J, Fokou I S M, Buckjohn C N D, Siewe M S and Tchawoua C 2020 *Physica A: Statistical Mechanics and its Applications* **557** 124857
[5] Yang T, Zhou S, Fang S, Qin W and Inman D J 2021 *Appl. Phys. Rev.* **8** 031317
[6] Harne R L and Wang K 2013 *Smart Materials and Structures* **22** 023001
[7] Dutoit N E, Wardle B L and Kim S G 2005 *Integrated Ferroelectrics* **71** 121
[8] Zhu H 2014 *Physica A* **410** 335
[9] Su M, Xu W and Zhang Y 2021 *Euro. Phys. J. Plus* **136** 271
[10] Zhu H 2014 *Journal of Sound and Vibration* **333** 954
[11] Jiang W A and Chen L Q 2013 *Mechanics Research Communications* **53** 85
[12] Li X, Yurchenko D, Li R, Feng X, Yan B and Yang K 2023 *Mechanical Systems and Signal Processing* **185** 109787
[13] Ghouli Z and Litak G 2023 *Journal of Vibration Engineering & Technologies* **11** 99
[14] Tang L, Yang Y and Soh C K 2010 *Journal of Intelligent Material Systems and Structures* **21** 1867
[15] Daqaq M F 2011 *Journal of Sound and Vibration* **330** 2554
[16] Stanton S C, McGehee C C and Mann B P 2010 *Physica D* **239** 640
[17] Cohen N, Bucher I and Feldman M 2012 *Mechanical Systems and Signal Processing* **31** 29
[18] Liu W, Badel A, Formosa F, Wu Y and Agbossou A 2013 *Smart Materials and Structures* **22** 035013
[19] Zheng R, Nakano K, Hu H, Su D and Cartmell M P 2014 *Journal of Sound and Vibration* **333** 2568
[20] Wang G, Liao W H, Yang B, Wang X, Xu W and Li X 2018 *Mechanical Systems and Signal Processing* **105** 427
[21] Yousefpour A, Haji Hosseinloo A, Reza Hairi Yazdi M and Bahrami A 2020 *Journal of Intelligent Material Systems and Structures* **31** 1495
[22] Guo Q, Sun Z, Zhang Y and Xu W 2019 *Complexity* **2019**
[23] Barton D A and Burrow S G 2011 *Journal of Computational and Nonlinear Dynamics* **6**
[24] Semenov V, Feoktistov A, Vadivasova T, Schöll E and Zakharova A 2015 *Chaos* **25** 033111
[25] Belhaq M, Ghouli Z and Hamdi M 2018 *Nonlinear Dynam.* **94** 2537
[26] Jin Y and Zhang Y 2021 *Acta Mechanica* **232** 1045
[27] Huan R, Zhu W, Hu R and Ying Z 2016 *Journal of Applied Mechanics* **83** 091009
[28] Xu P, Jin Y and Xiao S 2017 *Chaos* **27** 113109
[29] Yang T and Cao Q 2019 *Nonlinear Dynam.* **96** 1511
[30] Zhang S, Zhang Y, Sun Z and Duan X 2020 *Complexity* **2020**
[31] De S L and Ali S F 2022 *IFAC-PapersOnLine* **55** 411
[32] Tran N, Ghayesh M H and Arjomandi M 2018 *International Journal of Engineering Science* **127** 162
[33] Li T, Qu S and Yang W 2012 *J. Appl. Phys.* **112** 034119
[34] Li H, Li R, Fang X, Jiang H, Ding X, Tang B, Zhou G, Zhou R and Tang Y 2019 *Nano Energy* **58** 447
[35] Zhou J, Jiang L and Khayat R E 2017 *J. Appl. Phys.* **121** 184102
[36] Li S, Sun L and Kong F 2019 *Shock and Vibration* **2019** 4038657
[37] Oumbé Tékam G, Kitio Kwuimy C and Woafo P 2015 *Chaos: An Interdisciplinary Journal of Nonlinear Science* **25** 013112
[38] Huang D, Zhou S, Li W and Litak G 2021 *Science China Technological Sciences* **64** 858
[39] Tuwa P R N, Molla T, Noubissie S, Kingni S T and Rajagopal K 2021 *International Journal of Nonlinear Mechanics* **137** 103818
[40] Yang Y G, Meng Y, Zeng Y H and Sun Y H 2023 *Chin. Phys. B* **32** 090201
[41] Fang S, Zhou S, Yurchenko D, Yang T and Liao W H 2022 *Mechanical Systems and Signal Processing* **166** 108419
[42] Mantegna R N, Spagnolo B, Testa L and Trapanese M 2005 *J. Appl. Phys.* **97** 10
[43] Jin Y, Xu W and Xu M 2005 *Chaos, Solitons and Fractals* **26** 1183
[44] Zhang X and Xu W 2007 *Physica A* **385** 95
[45] Fu H, Mei X, Yurchenko D, Zhou S, Theodossiades S, Nakano K and Yeatman E M 2021 *Joule* **5** 1074
[46] Lei Y, Qiao Z, Xu X, Lin J and Niu S 2017 *Mechanical Systems and Signal Processing* **94** 148
[47] Li J, Zhang J, Li M and Zhang Y 2019 *Mechanical Systems and Signal Processing* **114** 128
[48] Zhang Y and Lei Y 2024 *Chin. Phys. B* **33** 038201
[49] Zhang Y, Zheng R, Kaizuka T, Su D, Nakano K and Cartmell M 2015 *Euro. Phys. J. Spec. Top.* **224** 2687
[50] Christensen R 2012 *Theory of viscoelasticity: an introduction* (Elsevier)
[51] Zhu W and Cai G 2011 *International Journal of Nonlinear Mechanics* **46** 720
[52] Zhang Y and Jin Y 2019 *Nonlinear Dynam.* **98** 501
[53] Zhang Y, Jin Y and Li Y 2021 *Physica D* **422** 132908
[54] Mann B and Owens B 2010 *Journal of Sound and Vibration* **329** 1215
[55] McInnes C, Gorman D and Cartmell M P 2008 *Journal of Sound and Vibration* **318** 655
[56] Shao R H and Chen Y 2009 *Physica A* **388** 977
[57] Gang H and Haken H 1990 *Phys. Rev. A* **41** 7078
[58] Gang H 1991 *Phys. Rev. A* **43** 700